NUCL SCI TECH (2016) 27:44
DOI 10.1007/s41365-016-0044-3

# Numerical analysis of the activity of irradiated alloy-N in an FHR

**Chao Peng[1,2] · Xing-Wang Zhu[1] · Guo-Qing Zhang[1] · Zhao-Zhong He[1] · Kun Chen[1]**

Received: 2 April 2015 / Revised: 1 June 2015 / Accepted: 1 June 2015 / Published online: 11 April 2016


**Abstract** The fluoride salt-cooled high-temperature reactor (FHR) uses molten FLiBe salt as the coolant, which introduces a corrosive effect on the alloy-N structure material. Fission neutrons activate the corroded alloy-N, along with alloy-N structures inside the reactor vessel. The activation products of the alloy-N have a big impact on radiation protection during operation, maintenance, and decommissioning of the reactor. We have constructed a SCALE 6.1 model for the core of a typical 10 $MW_{th}$ FHR and analyzed the activity of each constituent of the irradiated alloy-N. The results show that the activity is predominantly due to short-lived $^{28}Al$, $^{60m}Co$, $^{56}Mn$, $^{51}Ti$, and $^{52}V$, as well as long-lived $^{60}Co$, $^{51}Cr$, $^{55}Fe$, $^{59}Fe$, and $^{54}Mn$. Furthermore, because of their relatively long half-life and high-energy γ-rays emissions, $^{60}Co$ and $^{54}Mn$ are the major contributors to the radiation source terms introduced by alloy-N activation. The yield of $^{60}Co$ and $^{54}Mn$ per unit mass of alloy-N under the current core design is $5.58 \times 10^5$ and $1.55 \times 10^3$ Bq $MWd^{-1}$ $g^{-1}$, respectively. The results of this paper, combined with future corrosion studies, may provide a basis for evaluating long-term radiation source terms of the primary loop salt and components.

Supported by the "Strategic Priority Research Program" of the Chinese Academy of Sciences (Grant No. XDA02050100).

✉ Kun Chen
chenkun@sinap.ac.cn

[1] Shanghai Institute of Applied Physics, Chinese Academy of Sciences, Shanghai 201800, China

[2] University of Chinese Academy of Sciences, Beijing 100049, China

**Keywords** FHR · Alloy-N · Corrosion · Neutron activation · $^{60}Co$ · TMSR

## 1 Introduction

The concept of the molten salt reactor originated from Oak Ridge National Laboratory in the 1950s [1] using fluoride salts as both a coolant and fuel. In 2003, a fluoride salt-cooled high-temperature reactor concept, or FHR, was proposed by American scientists [2, 3]. The Center for Thorium Molten Salt Reactor System (TMSR) of the Chinese Academy Sciences (CAS) adopted the FHR concept and developed conceptual designs for test reactors in 2012 [4, 5]. As with other FHRs, the TMSR's design uses the TRISO (Tri-structural Isotropic) coated-particle fuel, molten FLiBe ($2LiF–BeF_2$) salt coolant, a graphite reflector, and alloy-N structural material, which has a high inherent safety under the design basis accidents, such as Loss Of Offsite Power (LOOP) accidents [6] and even Station Blackout Anticipated Transient Without Scram (SBO-ATWS) accidents [7].

The activation of the alloy-N by fission neutrons has a significant impact on the maintenance and decommissioning of the reactor. The alloy-N may be corroded and dissolved in the molten FLiBe salt and then irradiated by fission neutrons when the salt flows through the core. The alloy-N inside the reactor vessel will be activated by fission neutrons directly and then corroded into the molten FLiBe salt. The activated alloy-N in the salt may be deposited back onto the inner surface of the primary loop components, which is made of alloy-N. The primary loop components, containing long-life activation products that emit high-energy γ-rays, pose threats to the workers' health

during maintenance and decommissioning. The activation of the primary loop salt has been studied before [8, 9].

The corrosion and deposition of alloy-N in the FLiBe salt is a complicated process involving many physical and chemical mechanisms such as intrinsic corrosion, corrosion by oxidizing contaminants, differential solubility, galvanic corrosion, and so on [10]. These topics are well beyond the scope of this paper. Instead, this paper focuses on analyzing the activation of unit mass alloy-N in the core. Once the corrosion process is characterized correctly by future works, the results of this paper can be used to calculate the radiation source terms of the components and salt to support radiation protection, operation, maintenance, and decommissioning planning.

## 2 The reactor core

The core of the TMSR's test reactor is an octagonal prism filled with fuel pebbles and graphite pebbles. The graphite pebbles are only at the bottom and the top of the core. Each fuel pebble has a diameter of 6 cm and contains an average of 11,660 TRISO particles in its fuel zone. Each fuel pebble contains 7 g of uranium and the $^{235}$U enrichment is 17 wt%. Each TRISO particle consists of a $UO_2$ fuel kernel and several coating layers. The TRISO particles are randomly dispersed in a graphite matrix fuel zone in the pebble. A hard graphite shell encloses the fuel zone.

The pebble bed is surrounded by graphite reflectors with an outer diameter of 260 cm and a height of 300 cm. The thicknesses of the graphite reflectors on the top of the core and below the core are 65 and 50 cm, respectively. Channels are distributed in the top and bottom reflectors to allow the molten salt to flow through. Channels for situating control rods, measurement instruments, and neutron sources are located in the radial reflectors. The design parameters are listed in Table 1 [4].

Alloy-N is a 70.01 % Ni–16.50 % Mo–7.03 % Cr nickel-based alloy whose nominal composition is shown in Table 2 [11]. Ni and Mo in alloy-N provide excellent resistance to molten fluoride salt corrosion. However, the other metallic alloying elements in alloy-N may suffer from corrosion [12, 13]. Since this paper focuses on analyzing the neutron activation in the core, a unit mass of one gram of alloy-N is used in the calculation. Alloy-N is assumed to be in the coolant and irradiated by the fission neutrons. After the irradiation, the activities of alloy-N are primarily due to the short-lived $^{28}$Al, $^{60m}$Co, $^{56}$Mn, $^{51}$Ti, and $^{52}$V, as well as the long-lived $^{60}$Co, $^{51}$Cr, $^{55}$Fe, $^{59}$Fe, and $^{54}$Mn. Table 3 shows the properties of these nuclides [14, 15].

## 3 SCALE model of the core

In the multi-group (MG) neutron transport calculations, the initial problem-independent MG libraries were generated from the Evaluated Nuclear Data File (ENDF/B) using a generic flux spectrum. Before being used in the MG neutron transport calculation, the problem-independent MG library must be corrected for space-dependent and resonance self-shielding effects based on the unit cell description. FHR, which uses the fuel pebble, has double heterogeneity. The TRISO particles embedded in the graphite matrix constitute the first level of heterogeneity and the fuel pebbles with the moderator and reflector form the second level heterogeneity. This double heterogeneity must be treated through the unit cell description in order to obtain the accurate problem-dependent MG library.

We have built a SCALE 6.1 [16] computer model for the reactor core in order to calculate the activation products of alloy-N. The main challenge in modeling the core is to properly treat the double heterogeneity, which can be completed by the DOUBLEHET module. According to the

**Table 1** Design parameters of the test reactor

| Parameter | Data | Parameter | Data |
|---|---|---|---|
| Thermal power | 10 MW | Uranium loading | 77.28 kg |
| TRISO packing factor | 7 % | Operation time | 180 day |
| Pebble packing factor | 64 % | Core diameter (height)[a] | 2.6 m (3 m) |
| $^{235}$U enrichment | 17 % | Reactor vessel diameter (height) | 2.7 m (5 m) |
| Kernel diameter | 0.25 mm | PrC/IPyC/SiC/OPyC[b], μm | 90/40/35/40 |
| Fuel zone diameter | 5 cm | Fuel pebble diameter | 6 cm |
| U loading per pebble | 7 g | Active core height | 185 cm |
| Active core volume | 1.95 m$^3$ | Thickness of top reflector | 65 cm |
| Thickness of bottom reflector | 50 cm | | |

[a] The diameter of core includes the reflector

[b] PrC/IPyC/SiC/OPyC stand for porous carbon, inner pyrolytic carbon, silicon carbon and outer pyrolytic carbon, respectively

**Table 2** Nominal compositions (wt%) of the alloy-N

| Element | Ni | Mo | Cr | Fe | Mn | Si | Al | Co | Cu | W | Ti |
|---|---|---|---|---|---|---|---|---|---|---|---|
| wt% | 70.01 | 16.50 | 7.03 | 4.24 | 0.50 | 0.32 | 0.19 | 0.20 | 0.35 | 0.5 | 0.16 |

**Table 3** Activation products of the alloy-N

| Activation products | Reactions | Activation cross section and half-life | Decay modes | Emitted particle energy (MeV) |
|---|---|---|---|---|
| $^{28}$Al | $^{27}$Al(n,γ)$^{28}$Al | $4.74 \times 10^{-2}$ b | β$^-$, γ | β$^-$: 2.86 (100 %) |
| | (thermal) | (2.24m) | | γ: 1.78 (100 %) |
| $^{60}$Co | $^{59}$Co(n,γ)$^{60}$Co | 4.26 b | β$^-$, γ | β$^-$: 0.318 (99.89 %) |
| | (thermal) | (5.27a) | | γ: 1.332 (99.98 %), 1.173(99.87 %) |
| $^{60m}$Co | $^{59}$Co(n,γ)$^{60m}$Co | 5.34 b | IT (99.76 %) | γ: 0.0069(26.49 %) |
| | (thermal) | (10.47m) | β$^-$ (0.24 %) | |
| $^{51}$Cr | $^{50}$Cr(n,γ)$^{51}$Cr | 3.17 b | EC | γ: 0.320(9.83 %) |
| | (thermal) | (27.7d) | | |
| $^{55}$Fe | $^{54}$Fe(n,γ)$^{55}$Fe | $4.55 \times 10^{-1}$ b | EC | MnKX: $5.95 \times 10^{-3}$ (25.7 %) |
| | (thermal) | (2.7a) | | |
| $^{59}$Fe | $^{58}$Fe(n,γ)$^{59}$Fe | $2.67 \times 10^{-1}$ b | β$^-$, γ | β$^-$: 0.273 (45.4 %), 0.466 (53.1 %) |
| | (thermal) | (44.63d) | | γ: 1.099 (56.5 %), 1.292 (43.3 %) |
| $^{54}$Mn | $^{54}$Fe(n,p)$^{54}$Mn | $3.72 \times 10^{-3}$ b | EC | γ: 0.835 (99.978 %) |
| | ($E_n > 1$ MeV) | (312.7d) | | |
| $^{56}$Mn | $^{55}$Mn(n,γ)$^{56}$Mn | 2.89 b | β$^-$, γ | β$^-$: 0.735 (14.6 %), 1.037 (27.9 %), 2.848 (56.3 %) |
| | (thermal) | (2.58h) | | γ: 0.847 (98.9 %), 1.811 (27.2 %), 2.133 (14.3 %) |
| $^{51}$Ti | $^{50}$Ti(n,γ)$^{51}$Ti | $3.57 \times 10^{-2}$ b | β$^-$, γ | β$^-$: 1.537 (8.1 %), 2.146 (91.9 %) |
| | (thermal) | (5.76m) | | γ: 0.32 (92.9 %), 0.929 (6.87 %) |
| $^{52}$V | $^{52}$Cr(n,p)$^{52}$V | $4.03 \times 10^{-5}$ b | β$^-$, γ | β$^-$: 2.54 (99.2 %) |
| | ($E_n > 4$ MeV) | (3.75m) | | γ: 1.43 (100 %) |

MnKX: X-ray produced by filling the K vacancy in the nuclide Mn

*IT* isomeric transitions, *EC* electron capture

unit cell described by the DOUBLEHET, SCALE uses the conventional Bondarenko method to process the shielding factors in the unresolved resonance range and a deterministic pointwise calculation of the fine-structure spectra in the resolved resonance and thermal energy ranges to generate the problem-dependent MG cross sections, which are then used to perform the depletion analysis.

The repeated structural unit chosen to build the active core consists of a pebble at the body-center of the cubic and a 1/8 pebble at every corner of the cubic. Figure 1 shows the repeated structural unit, which has the same length and width of 7 cm and a height of 6.78 cm, which maintains a pebble packing factor of 64 %. These repeated structural units are arranged in an infinite square lattice and enclosed by an octagonal prism to form the active core. The pebbles in contact with the surfaces of the octagonal prism may be cut. Several types of special structural units have been used to replace the repeated structural units, which stay within

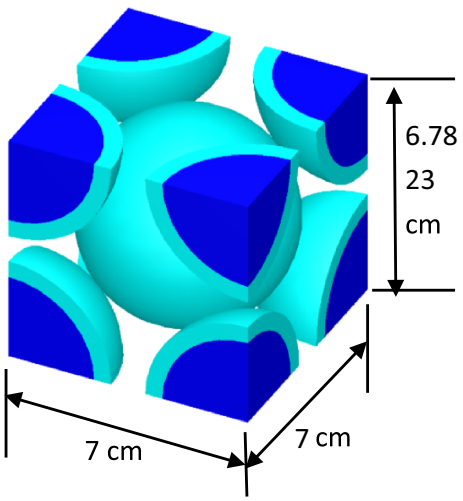


**Fig. 1** The repeated structural unit to form the active core

the boundary of the core to ensure one whole pebble stays within the boundary.

A model of the core is shown in Fig. 2. The shutdown and control system channels are included in the model but filled with a vacuum. That is to say, the control and shutdown rods are assumed to be fully withdrawn from the core. The boundary condition of the model is set to be a vacuum.

The control module, TRITON, of SCALE 6.1 is used to calculate the activity of the activation products. KENO-VI performs neutron transport analysis and is coupled with the ORIGEN module to perform the depletion calculations. The cross section library of v7-238 is used, and the CENTRM module is used for cross section processing.

## 4 Results and discussion

### 4.1 Neutron spectrum

The activation products, such as $^{28}$Al, $^{60m}$Co, $^{56}$Mn, $^{51}$Ti, $^{60}$Co, $^{51}$Cr, $^{55}$Fe, and $^{59}$Fe, are produced by thermal neutron capture reactions. However, $^{54}$Mn and $^{52}$V are produced by fast neutron (n, p) reactions. Thus, the neutron spectrum may significantly affect the production of the activation products. Since the alloy-N is dissolved in the coolant, the neutron spectrum averaged over the coolant in the core is of great interest, and the neutron spectrum at the beginning of the cycle is shown in Fig. 3. The spectrum is calculated using the model described in Sect. 3. The reactor has a thermal neutron spectrum and the ratio of thermal flux to total flux is approximately 40 %.

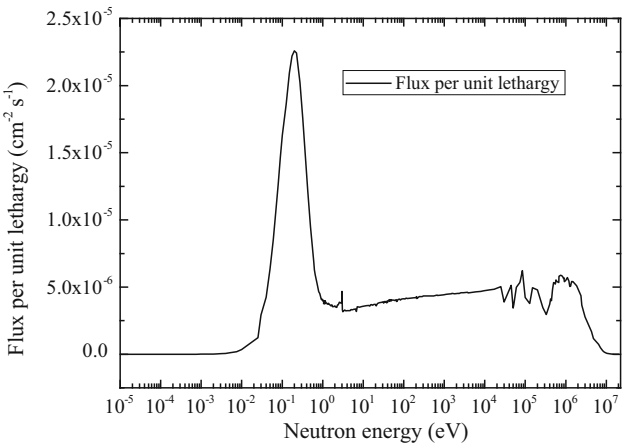


**Fig. 3** Neutron spectrum averaged over the coolant in the core at the beginning of the cycle

### 4.2 Activity of alloy-N

#### *4.2.1 Activity in power operation*

Activities of the alloy-N per unit mass after the reactor runs at full power for 180 days are listed in Table 4. Activities of each activation product changing with the irradiation time are shown in Fig. 4. Short-lived nuclides such as $^{28}$Al, $^{60m}$Co, $^{56}$Mn, and $^{51}$Ti reach their maximum activities before the end of the cycle due to their very short half-life. However, $^{52}$V, a very short-lived nuclide, does not reach its maximum activity immediately because of the small activation cross section of $^{52}$Cr to produce $^{52}$V. Long-lived nuclides such as

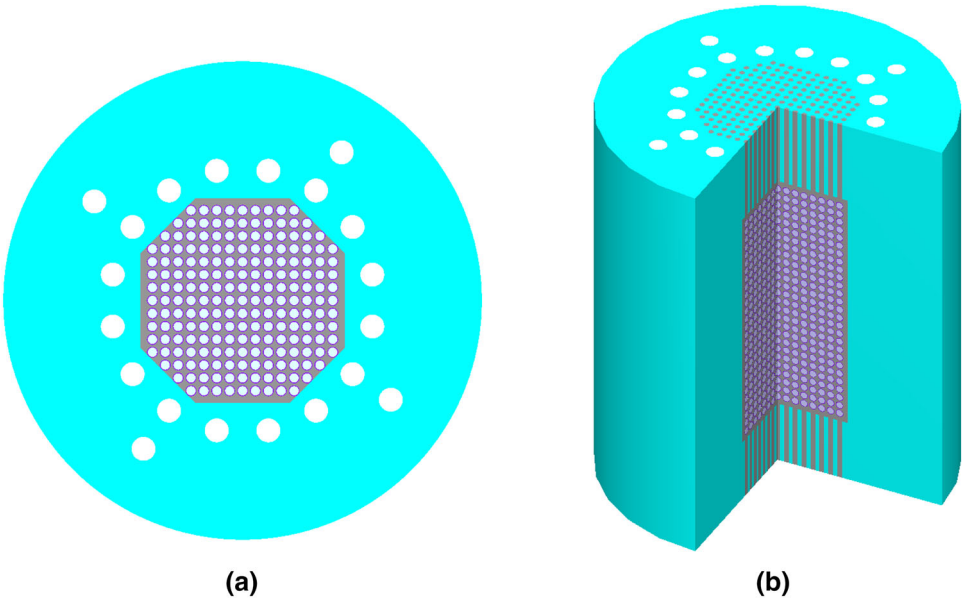


**Fig. 2** Model of the core: **a** cross section; **b** three-quarters of the total profile

**Table 4** Activities of alloy-N per unit massat the end of the cycle

| Nuclide | Activity (Bq/g) | Nuclide | Activity (Bq/g) |
|---|---|---|---|
| $^{56}$Mn | 1.33E+10 | $^{28}$Al | 1.70E+08 |
| $^{51}$Cr | 9.20E+10 | $^{59}$Fe | 2.70E+07 |
| $^{60m}$Co | 9.15E+09 | $^{52}$V | 1.18E+07 |
| $^{60}$Co | 1.00E+09 | $^{54}$Mn | 2.78E+06 |
| $^{55}$Fe | 1.16E+08 | $^{51}$Ti | 3.16E+06 |

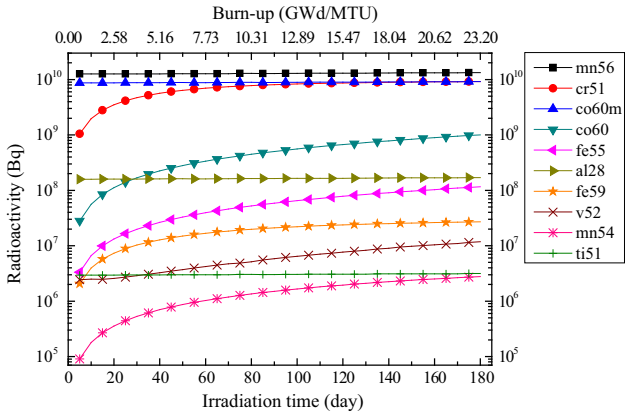


**Fig. 4** Activities of the activation products changing with the irradiation time

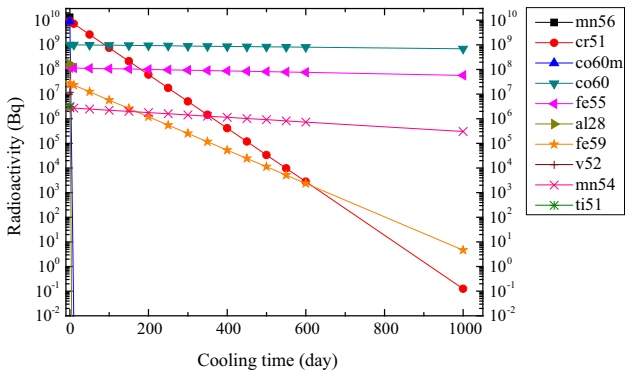


**Fig. 5** Activities of the activation products after shutdown

$^{60}$Co, $^{51}$Cr, $^{55}$Fe, $^{59}$Fe, and $^{54}$Mn reach their maximum activities at the end of the cycle. The nuclides of $^{56}$Mn, $^{60}$Co, $^{28}$Al, $^{59}$Fe, $^{52}$V, and $^{54}$Mn undergo $\beta^-$ and $\gamma$ decay by emitting high-energy $\gamma$-rays. Thus, in the power operation of the reactor, $^{56}$Mn, $^{60}$Co, $^{28}$Al, $^{59}$Fe, $^{52}$V, and $^{54}$Mn may be important in terms of radiation protection.

### *4.2.2 Activity after shutdown*

After the shutdown of the reactor, the activity decreases due to decay. Activities decreasing with the cooling time are shown in Fig. 5. The short-lived nuclides of $^{28}$Al, $^{60m}$Co, $^{56}$Mn, $^{51}$Ti, and $^{52}$V die out in a few days, and the long-term radiation source terms are primarily due to the long-lived nuclides of $^{60}$Co, $^{55}$Fe, $^{54}$Mn, $^{51}$Cr, and $^{59}$Fe. However, $^{55}$Fe and $^{51}$Cr undergo electron capture and emit very low-energy x-rays and $\gamma$-rays. Thus, the radiation source terms of the irradiated alloy-N are mainly due to $^{60}$Co, $^{54}$Mn, and $^{59}$Fe. The nuclides of $^{60}$Co, with a half-life of 5.72 years, undergo $\beta^-$ decay and emit two $\gamma$-rays with energies of 1.17 and 1.33 MeV, respectively. The nuclides of $^{54}$Mn, with a half-life of 312 days, undergo electron capture and emit 0.835 MeV $\gamma$-rays. The nuclides of $^{59}$Fe, with a half-life of 44.63 days, undergo $\beta^-$ decay and emit two $\gamma$-rays with energies of 1.099 and 1.292 MeV, respectively. Furthermore, due to their long half-life, the activities of $^{60}$Co and $^{54}$Mn increase with the irradiation time almost linearly. The production rates of $^{60}$Co and $^{54}$Mn per unit mass of alloy-N are $5.58 \times 10^5$ and $1.55 \times 10^3$Bq MWd$^{-1}$ g$^{-1}$, respectively.

In addition, attention should be paid to $^{60m}$Co. $^{60m}$Co undergoes isomeric transition and $\beta^-$decay with a branching ratio of 99.76 and 0.24 %, respectively. Its isomeric transition produces $^{60}$Co, which is a main contributor to the radiation source terms.

## 5 Conclusion

We have constructed a SCALE 6.1 model for the TMSR's test reactor core and used the model to calculate the average neutron spectrum in the coolant. We also used the model to calculate and analyze the activity of each constituent in the irradiated alloy-N. The results show that among the activation products, $^{60}$Co and $^{54}$Mn, which emit high-energy $\gamma$-rays, are the major contributors to the radiation source terms considering their relatively long half-life. Because of the corrosion of alloy-N by the FLiBe salt, the activation products of the alloy-N may be dissolved in the coolant and deposited onto different components of the primary loop. The exact corrosion and mass transport process is yet to be understood. Nevertheless, the salt and components may be highly radioactive after a prolong power operation, even after a long cooling time, because of the existence of $^{60}$Co. This is a unique situation for FHRs and may complicate maintenance and decommissioning. Therefore, it is important to quantify the activation of alloy-N in the primary loop. This paper is the first step in analyzing the activation of alloy-N in FHRs.

## References

1. W.B. Cottrell, H.E. Hungerford, J.K. Leslie, et al. *Operation of the Aircraft Reactor Experiment*. Oak Ridge National Laboratory, ORNL-1845 (1955)

2. C.W. Forsberg, P.F. Peterson, P.S. Pickard, Molten-salt-cooled advanced high-temperature reactor for production of hydrogen and electricity. Nucl. Technol. **144**, 289–302 (2003)
3. C. Forsberg, L.W. Hu, P. Peterson, et al. *Fluoride-Salt-Cooled High-TEMPERATURE REACTORS (FHRs) for Power and Process Heat*. MIT-ANP-TR-157 (2014)
4. TMSR-SF1 Neutron Physics Parameters. Center for Thorium Molten-salt Reactor System, XD02010200-TL-2013-11 (internal technical report) (2013)
5. M.H. Jiang, H.J. Xu, Z.M. Dai, Advanced fission energy program-TMSR nuclear energy system. Bull. Chin. Acad. Sci. **27**, 366–374 (2012). doi:10.3969/j.issn.1000-3045.2012.03.016
6. M.D. Mei, S.W. Shao, J.X. Zuo et al., Probability safety assessment of LOOP accident to molten salt reactor. Nucl. Technol. **36**(12), 56–63 (2013). **(in Chinese)**
7. X.W. Jiao, K. Wang, Z.Z. He et al., Core safety discussion under station blackout ATWS accident of solid fuel molten salt reactor. Nucl. Technol. **38**, 79–85 (2015). doi:10.11889/j.0253-3219.2015.hjs.38.020604
8. X.W. Zhu, S. Wang, C. Peng, et al. *The Analysis of Tritium Generation in the Solid Fuel Thorium Molten Salt Reactor* in *Transactions of the American Nuclear Society*, Washington (2013)
9. X.W. Zhu, S. Wang, C. Peng et al., Production and release of 14C in TMSR-SF1. Nucl. Tech. **38**, 30603 (2015). doi:10.11889/j.0253-3219.2015.hjs.38.030603
10. M.S. Sohal, M.A. Ebner, P. Sabharwall, et al. *Engineering Database of Liquid Salt Thermophysical and Thermochemical Properties*. Idaho National Laboratory, Idaho Falls, INL/EXT-10-18297 (2010)
11. G.Q. Zhang, X.W. Zhu, X.W. Guo, et al. *Preliminary Analysis of Radioactive Source Terms of TMSR-SF1*. Shanghai Institute of Applied Physics, TMSR-NE-RS-TR-2014-19 (internal technical report) (2014)
12. R.B. Briggs. *Molten-Salt Reactor Program Semiannual Progress Report for Period Ending February 28, 1962*. Oak Ridge National Laboratory, ORNL/TM-3282 (1962)
13. R.S. Sellers. *Impact of Reduction-Oxidation Agents on the High Temperature Corrosion of Materials in LiF-NaF-KF*. Ph.D. Thesis, University of Wisconsin-Madison (2012)
14. M.F. L'Annunziata. *Chapter 1—Radiation Physics and Radionuclide Decay*, in *Handbook of Radioactivity Analysis*, 3rd edn. ed. by M.F. L'Annunziata (Academic Press, Amsterdam, 2012), pp. 1–162
15. G. Audi, O. Bersillon, J. Blachot et al., The nubase evaluation of nuclear and decay properties. Nucl. Phys. A **729**, 3–128 (2003). doi:10.1016/j.nuclphysa.2003.11.001
16. *Scale: A Comprehensive Modeling and Simulation Suite for Nuclear Safety Analysis and Design*. ORNL/TM-2005/39, Version 6.1, June 2011, Available from Radiation Safety Information Computational Center at Oak Ridge National Laboratory as CCC-785